JACS
JOURNAL OF THE AMERICAN CHEMICAL SOCIETY

COMMUNICATION

pubs.acs.org/JACS

Chain-Branching Control of the Atomic Structure of Alkanethiol-Based Gold−Sulfur Interfaces

Yun Wang,[†] Qijin Chi,[‡] Jingdong Zhang,[‡] Noel S. Hush,[§,⊥] Jeffrey R. Reimers,*[,⊥] and Jens Ulstrup[‡]

[†]Centre for Clean Environment and Energy, Griffith School of Environment, Griffith University, Gold Coast, QLD 4222, Australia
[‡]Department of Chemistry and NanoDTU, Technical University of Denmark, DK-2800 Lyngby, Denmark
[§]School of Molecular Biosciences and [⊥]School of Chemistry, The University of Sydney, NSW 2006, Australia

Supporting Information

ABSTRACT: Density functional theory structure calculations at 0 K and simulations at 300 K of observed high-resolution *in situ* scanning tunneling microscopy (STM) images reveal three different atomic-interface structures for the self-assembled monolayers (SAMs) of three isomeric butanethiols on Au(111): direct binding to the Au(111) surface without pitting, binding to adatoms above a regular surface with extensive pitting, and binding to adatoms with local surface vacancies and some pitting. Thermal motions are shown to produce some observed STM features, with a very tight energy balance controlling the observed structures. Variation of the degree of substitution on the α carbon is found to significantly change the relative energies for interaction of the different types of adatom structures with the surface, while the nature of the surface cell, controlled primarily by inter-adsorbate steric interactions, controls substrate reorganization energies and adsorbate distortion energies. Most significantly, by manipulating these features, chemical control of the adsorbate can produce stable interfaces with surface pitting eliminated, providing new perspectives for technological applications of SAMs.

Devices for use in molecular electronics and as biosensors are often fabricated using self-assembled monolayers (SAMs) of thiols or disulfides on gold surfaces.[1,2] Similar chemistry is also used to stabilize gold nanoparticles.[3] The fluidity of gold surfaces can be a problem,[4,5] but some structures are very stable. Controlling the atomic structure of gold−sulfur interfaces is therefore an important aspect of any technological application.

In principle, many factors determine the structure of the SAM, including the metal−headgroup interaction, interactions between the adsorbate molecules, and solvation of the adsorbates; here we focus on the intermolecular interactions. Three chemisorbed isomeric alkanethiols, 1-butanethiol (linear chain, **L**),[6] 2-methyl-1-propanethiol (branched chain, **B**),[7] and 2-methyl-2-propanethiol ("tree-like" maximally branched chain, **T**)[8,9] (see Scheme 1), of increasing lateral area and steric demands are used to demonstrate chemical control to produce an intriguing diversity of interfacial structures. Results from scanning tunneling microscopy (STM) imaging[6−8] are interpreted using room-temperature density functional theory (DFT) simulations to show that the atomic structures of the interfaces formed are of three qualitatively different types. The bonding features responsible for these differences are elucidated using low-temperature

Scheme 1. Molecular Structures of Methanethiol (M) and Isomeric Alkanethiols 1-Butanethiol (L), 2-Methyl-1-propanethiol (B), and 2-Methyl-2-propanethiol (T)

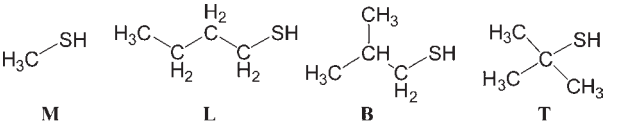

simulations for these adsorbates as well as for methanethiol (**M**) SAMs (Scheme 1), as is the difference in bonding between surface monolayers and nanoparticle coverings.

During chemisorption of thiols on gold, the thiol hydrogen is lost, leaving an electrically neutral alkylthiyl radical ($RS^{\bullet}$) that covalently adsorbs to the surface.[7,10−11] Early structural studies considered the binding as occurring via simple addition to the unreconstructed Au(111) surface.[10,12−13] However, the sulfur adsorption site was predicted by calculations to be quite different from that observed spectroscopically,[13−14] and the original structural model could not account for surface pitting.[15] As a result, alternative binding models have been recently proposed, among which the most successful is one with two chemisorbed alkanethiol molecules attached to the surface as well as to a supersurface gold adatom "mined" out of the surface in an RS-Au-SR configuration;[3,7,16−20] other postulates[21] include Au-SR supersurface structures.[22]

Direct observation of adatom-bound adsorbates on Au(111) using STM has been reported for methanethiol SAMs at both low[17] and high[16] coverage in vacuum. Also, adatom-mediated motifs have been observed in thiol monolayer-covered gold clusters through X-ray diffraction experiments.[3] Adatoms on the surface are also apparent from careful removal of the adsorbates[18] using hydrogen adsorption and desorption techniques[19] and from solution STM.[6,7]

Assembly of most thiol monolayers on gold is accompanied by the formation of pits, a process that yields gold adatoms for the interface. Not all required adatoms originate from pits, however, other sources including the mining of terrace edges, extraction of isolated individual atoms from the top surface layer to form local vacancies,[6,7,11,15,16,20,23] and utilization of atoms released by the lifting of the Au(111) surface reconstruction[6,24] (liberating 4.5% of a monolayer of Au atoms). Quantification of the density of gold adatoms is possible, providing crucial clues for understanding SAM interface structures. Recent experimental *in situ* STM studies[6−8] in solution on single-crystal gold samples under electrochemical control

Received: May 30, 2011
Published: August 22, 2011

have yielded high-resolution images for the **L**, **B**, and **T** isomers, and representative images are shown in Figure 1. Under these conditions, large Au(111) terraces are produced, minimizing contributions from edge mining to adatom supply. As a result, the observed pit density, given in Table 1, pertains directly to the chemisorption process. The observed supersurface SAM lattice vectors and the coverage determined electrochemically are also given in this table.

Unfortunately, these STM images directly reveal neither the number or location of adatoms in the surface cells nor the concentration of isolated vacancies in the top surface layer.[6,7] DFT-based STM image simulations at 0 K for a large number of possible structures have indicated likely candidates,[6,7,9] but it is clear that the large conformational space possessed by these molecules, combined with variations in surface structure, render these results as indicative only.[20] Here, we perform additional searches for low-energy structures of chemisorbed **T** and, for all adsorbates, molecular dynamics simulations[25] at T = 300 K. The VASP electronic structure program[26] is used along with the PW91 density functional,[27] and STM images are simulated at both 0 and 300 K; details of these calculations are provided in the Supporting Information (SI); established procedures are used.[9,11] Note that all previously identified 0 K structures are reoptimized at a consistent, high level of theory, with particular attention paid to finding the lowest-energy conformers and generating high-precision results.

The observed STM images are compared to those simulated at both 0 and 300 K in Figure 1. For both **L** and **B** thermal effects are significant, indicating that dynamical processes such as chain disordering can control image details.[20] The high-temperature simulations describe the strikingly different locations and intensity patterns found in the observed images.

As is apparent from the sample structures shown in Figure 1, isomeric changes in the molecular structure confer quite different apparent surface areas to the alkyl chains. This results in the quite different coverages of 1/3, 1/4, and 1/7 $RS^{\bullet}$ radicals per Au(111) surface gold atom for **L**, **B**, and **T**, respectively (Table 1). The supersurface lattice vectors also show significant changes in shape, from the nearly square $(3\times2\sqrt{3})$-4 lattice for **L** via the highly rectangular $(8\times\sqrt{3})$-4 lattice for **B** to the rhombic $(2\sqrt{7}\times\sqrt{7})$-2 lattice for **T**.

The observed degree of surface pitting also shows considerable variation,[6−8] increasing from 4.0% for **L** to 5.6% for **B**, while no pitting is observed for **T** (Table 1) and that for **M** is estimated at 12−20%. For **M** and **B**, the pit coverage indicates that the SAM is bound to adatoms as RS-Au-SR above a regular Au(111) surface, a result which is supported by the simulated STM images. For **L**, the observed coverage indicates that either half the adsorbates are so bound to adatoms with the other half bound directly, or else all adsorbates are bound as RS-Au-SR with also one local vacancy in the surface layer of the unit cell. Only the simulated STM image arising from the local-vacancy model is consistent with the observed image, however. For **T**, the absence of surface pits indicates that either all adsorbates are bound directly to the surface, as previously concluded,[9] or else all are bound to adatoms with compensating local surface vacancies. The observed STM images are inconsistent with RS-Au-SR

Table 1. Properties[a] of SAMs of Methanethiol (M), 1-Butanethiol (L), 2-Methyl-1-propanethiol (B), and 2-Methyl-2-propanethiol (T) at Full-Monolayer Coverage

property	M	L	B	T
% pits	12−20	4.0	5.6	0
coverage	1/3	1/3	1/4	1/7
lattice	$(3\times2\sqrt{3})$-4	$(3\times2\sqrt{3})$-4	$(8\times\sqrt{3})$-4	$(2\sqrt{7}\times\sqrt{7})$-2
adatoms	2	2	2	0
vacancies	0	1	0	0
adsorbate str.	adatom *cis*	adatom *cis*	adatom *trans*	monomers
ΔE	−1.75	−1.73	−1.69	−1.65
ΔE (RSSR)	−0.78	−0.76	−0.73	−0.55
ΔE_{nxt}	0.02[b,d]	−0.03[b,d]	0.02[b,d]	−0.01[b,d]
ΔE_{pit}	0.02[c]	0.04[b]	−0.01[c]	−0.20
$\Delta E_{pit,substrate}$	−0.47	−0.51	−0.45	−0.46
$\Delta E_{pit,adatom\ cplx}$	0.00	0.00	0.08	0.00
$\Delta E_{pit,interaction}$	0.46	0.55	0.36	0.26
α	59.5, 59.8	60.0, 60.4	60.5, 61.3	63.1

[a] Observed[6−8] pit coverage, thiol coverage, and lattice parameters; the deduced[6−8] numbers of adatoms and vacancies and adsorbate configuration; and at T = 0 the calculated energy of binding of alkanethiyl radicals ΔE and disulfides ΔE(RSSR) (eV per adsorbate), the relative energy of the closest alternative structure ΔE_{nxt} (eV), energy of transferring a localized gold vacancy into a pit ΔE_{pit} and its substrate and adatom components and interaction energy (eV), and Au−Au(adatom)−Au angle α (°) for the lowest-energy adatom-bound structure. [b] Obs > 0. [c] Obs < 0. [d] Relative energy of alternative nonobserved configuration with adatom:vacancy ratios of 2:1 for **M**, 2:0 for **L**, 2:2 for **B**, and 1:0 for **T**.

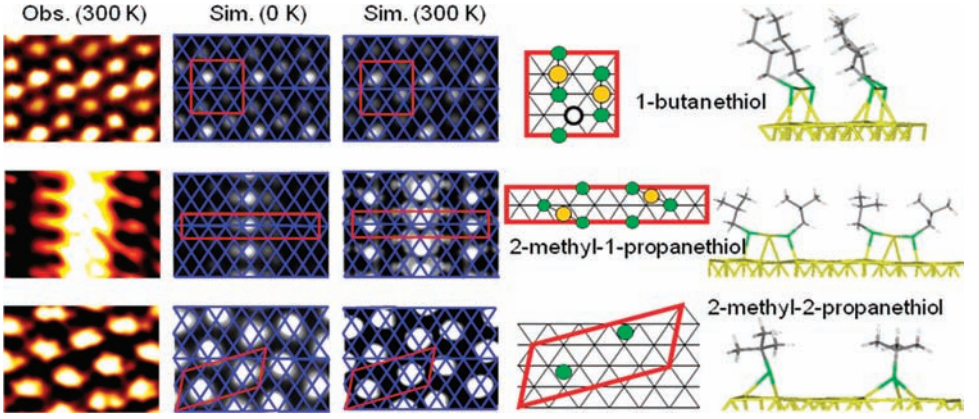

Figure 1. Observed[6−8] and simulated STM images for the SAMs of 1-butanethiol, 2-methyl-1-propanethiol, and 2-methyl-2-propanethiol on Au(111) surfaces. In these STM images, superimposed blue lines indicate the gold substrate lattice, while red lines indicate the SAM surface lattices. Atom color code: yellow, gold; green, sulfur; gray, carbon; white, hydrogen; black open circle; gold surface-layer vacancy.

dx.doi.org/10.1021/ja204958h |*J. Am. Chem. Soc.* 2011, 133, 14856–14859

binding but could, in principle, be explained by other options previously unexplored for this system, such as Au-SR or RS-Au-Au-SR binding. A total of 227 possible structures containing these features, that are also likely to be consistent with the observed STM images, were simulated, and the lowest-energy forms identified for four structural types are detailed in the SI. Per adsorbate, these structures were calculated to be at least 0.63 eV (for RS-Au-Au-SR) or 0.76 eV (for Au-SR) less stable than binding without adatoms to a flat surface, however, supporting the existing structural model.[9]

As highlighted in Table 1, the three isomers thus produce three different interface topologies, resulting in three different C−S arrangements,[28] identified from the simulations to be *cis* across the adatom for **L**, *trans* for **B**, and independent (no adatom) for **T**.

Table 1 shows the calculated energies ΔE for the reaction of the alkanethiyl radicals RS$^\bullet$ to form adsorbates at their deduced structures, as well as the related disulfide adsorption energies ΔE(RSSR). ΔE ranges from −1.75 eV for **M** and −1.73 eV for **L** to −1.65 eV for **T**. The observed[29] activation enthalpies for desorption of **L** and **T** are 1.32 and 1.11 eV, respectively; these are much less than the calculated $-\Delta E$ values as they pertain to low-density SAMs (e.g., $(23\times\sqrt{3})$-4 for the octanethiol SAM[30] and $(12\times\sqrt{3})$-2 for the undecanethiol SAM[31]) at the desorption temperature of ∼475−525 K, but the observed lower stability of the **T** SAM is qualitatively reproduced by the calculations. Note that Au_{27} cluster calculations for the binding site performed using GAUSSIAN09[32] indicate only minor zero-point energy corrections (∼ 0.06 eV), and net thermal corrections (∼0.03 eV) contribute to these enthalpy changes (see SI).

While calculated energies have been shown to be very useful in discriminating between alternate structural possibilities, complete *a priori* prediction of the observed structure is not possible. A variety of structures are actually predicted to have energies very similar to ΔE as reported for the observed structure in Table 1. The observed structure is, however, found to be either the lowest-energy one calculated or else the second-lowest-energy one, with the magnitude of the energy difference ΔE_{nxt} between the two lowest-energy structures being at most 0.03 eV, well below the accuracy of the calculations. For all adsorbates, only one low-energy structure is consistent with both the observed pit coverages and STM images, however.

For **M**, **L**, and **B**, the two lowest-energy structures differ by the location of the surface atoms mined to form adatoms: either local vacancies within the unit cell or else these vacancies coalesced into pits. An important aspect of our calculations is thus the energy required to extract a gold atom from a pit. As detailed in the SI, we crudely estimate this[7] to be 3.38 eV by removing two adjacent surface rows from the $(8\times\sqrt{3})$ surface.

For each adsorbate, the energy of moving a localized gold vacancy into a surface pit, ΔE_{pit}, is given in Table 1, along with its decomposition into three contributions: the energy from the reorganization of the substrate, $\Delta E_{pit,adatom\ cplx}$, the reorganization of the associated RS-Au-SR adatom complex, $\Delta E_{pit,substrate}$, and the interaction energy between the adatom complex and the substrate, $\Delta E_{pit,interaction}$. The substrate energy changes are all large and negative, ranging from −0.45 to −0.51 eV, indicating that gold strongly prefers to have agglomerated pits in its surface rather than distributed local vacancies. In contrast, almost no change in the energy of the adatom complex on vacancy transfer is found, the only noticeable contribution being 0.08 eV for **B** arising owing to the sterically compressed nature of the SAM and the additional freedom offered by the local vacancy structure.

Table 2. Properties[a] of SAMs of 1-Butanethiol (L), 2-Methyl-1-propanethiol (B), 2-Methyl-2-propanethiol (T), and Methanethiol (M) at Low Coverage for Direct Monomer Adsorption without Surface Rearrangement and after Surface Atom Extraction To Form an Adatom with Adjacent Vacancy (AV)-Bound Adsorbate Dimer

property	surface	M	L	B	T
no. $C_\alpha-C_\beta$ bonds		0	1	1	3
ΔE_{direct}	un-recon[b]	−1.61	−1.59	−1.57	−1.62
ΔE_{AV}	un-recon[b]	−1.58	−1.59	−1.54	−1.57
$\Delta E_{extract}$	un-recon[b]	0.03	0.00	0.03	0.05
θ_{direct}	un-recon[b]	58, 48	58,45	58, 47	16, 7
θ_{AV}	un-recon[b]	51, 51	59, 49	61,47	46, 42
ΔE_{direct}	recon[c]	−1.66	−1.68	−1.69	−1.76
ΔE_{AV}	recon[c]	−1.85	−1.80	−1.78	−1.72
$\Delta E_{extract}$	recon[c]	−0.18	−0.12	−0.08	0.04
θ_{direct}	recon[c]	19, 7	18, 7	8, 2	6, 2
θ_{AV}	recon[c]	58, 50	54, 48	51, 51	58, 45
height (AV C_β)	recon[c]	–	3.45	3.50	3.29

[a] Calculated binding energies ΔE (in eV per adsorbate radical), $S-C_\alpha$ vector orientations θ to the surface normal (degrees), and height of the closest C_β atom above the surface (Å). [b] At $\Theta = 1/12$ on a $(6\times2\sqrt{3})$-2 lattice. [c] At $\Theta = 1/44$ on a $(22\times2\sqrt{3})$-2 lattice.

Finally, the changes in interaction energy between the adatom complexes and the surface are found to vary significantly from 0.26 eV for **T** to 0.55 eV for **L**; these large positive values indicate that the RS-Au-SR complex much prefers to bind to a surface containing local vacancies than to a regular (111) surface. For **M**, **L**, and **B**, the two large effects of substrate relaxation and adatom−complex interaction essentially cancel, giving small total energies for transferring a local vacancy to a pit of ΔE_{pit} = −0.01 to 0.04 eV, ordered correctly according to the results implied from the experimentally observed structures. These results thus give qualitative support to the adatom:vacancy ratios of 2:0, 2:1, and 2:0, observed for **M**, **L**, and **B**, respectively.

In a second set of calculations of structures at low coverage appropriate for $T = 0$ K, we examine in particular the influence of the headgroup interaction on the ability of a SAM to extract adatoms from a surface to form an adatom complex with localized cell vacancy. The effects of the varying coordination to the C_α atoms are summarized in Table 2 and described in detail in the SI. We consider only adsorbates at low coverage both on a regular Au(111) surface and on the bare reconstructed surface that is present in the experiments before thiols are added. On each type of surface, Table 2 shows the energy of direct binding ΔE_{direct} to the surface without gold atom rearrangements, the associated energy ΔE_{AV} to form a modified structure with one adatom complex and one local vacancy per cell, and the gold atom extraction energy $\Delta E_{extract}$, being the difference between these quantities. The coverages modeled are $\Theta = 1/12$ on the unreconstructed surface and $\Theta = 1/44$ on the reconstructed one, a coverage that is expected to be far too low to facilitate lifting of the reconstruction.[11]

The tertiary alkanethiol **T** is calculated to bind slightly more strongly to the flat, un-reconstructed surface than either **M**, **L**, or **B** but to bind significantly more strongly to the flat, reconstructed surface. This is unexpected in that steric repulsions force **T** to chemisorb with nearly vertical $S-C_\alpha$ bonds ($\theta = 7°$ and 16° in Table 2), whereas the other adsorbates form in a more stable

configuration, with these bonds tilted with $45° < \theta < 58°$, indicating that the binding strength is quite sensitive to the nature of the carbon bonded to the sulfur. However, this effect mostly operates in the opposite direction for binding to an adatom with adjacent local vacancy, causing the tertiary alkanethiol to bind less strongly. As a result, the energies for extraction of an adatom are −0.18, −0.12, −0.08, and 0.04 eV for **M**, **L**, **B**, and **T**, respectively, on the reconstructed surface. Note that while Table 2 shows that chemical coordination forces C_β atoms slightly closer to the surface for adatom-bound **T**, the separation remains ca. 3.3 Å where there is insufficient steric repulsion to influence energetics.

A protocol thus emerges for understanding interface structures at the atomic scale: (1) increasing the degree of substitution on C_α significantly influences the interactions of the adsorbates with the surface, with extensive substitution favoring adsorption to flat surfaces over adsorption to adatom complexes with local vacancies over adsorption to adatom complexes with coalesced pits, and (2) steric interactions between the molecular adsorbates determine the surface unit cell and hence influence intra-substrate interactions at high coverage and possibly also give rise to steric effects. As shown in Figure 1, the $(3\times2\sqrt{3})$-4 lattice found generally for **M** and linear alkanethiols such as **L** is particularly suited to stabilizing loca vacancy structures, as the local vacancy is located adjacent to three surface gold atoms that are vertically attached to sulfur, maximizing adsorbate stabilization.

A generally important property for adatom-bound species without local vacancies is the Au−Au(adatom)−Au angle, where the outside gold atoms are on the surface. For all structures considered at low coverage (see SI), one of these two outside surface atoms is missing, suggesting that this structural aspect provides a weakness to the overall bonding. For the high-coverage structures of **M**, **L**, and **B** described in Table 1, this is 60−61°, increasing to 63° for the lowest-energy adatom-bound structure found for **T**. However, on the $Au_{102}(SC_6H_4{-}COOH)_{44}$ nanocluster,[3] this angle increases to 85°, relaxing the calculated energy[11b] of the adatom-bound motif by 0.25 eV. This change is comparable with the subtle variations found for adsorbates on Au(111) and is responsible for the dominance of adatom-bound adsorbates on nanoclusters.

In summary, by considering isomeric adsorbates with very different adsorbate cross sections, we have shown that a range of interface structures between organic sulfur and gold surfaces can be established and controlled. In particular, undesirable interface features such as surface pitting can be eliminated, making more regular structures for device applications.

■ ASSOCIATED CONTENT

Supporting Information. Computation modeling, optimized structures, and complete ref 32. This material is available free of charge via the Internet at http://pubs.acs.org.

■ AUTHOR INFORMATION

Corresponding Author
jeffrey.reimers@sydney.edu.au

■ ACKNOWLEDGMENT

We thank the Australian Research Council, National Computer Infrastructure, and Intersect as well as the Danish Research Council for Technology and Production Science.

■ REFERENCES

(1) Love, J. C.; Estroff, L. A.; Kriebel, J. K.; Nuzzo, R. G.; Whitesides, G. M. *Chem. Rev.* **2005**, *105*, 1103.
(2) Zhang, J.; Kuznetsov, A. M.; Medvedev, I. G.; Chi, Q.; Albrecht, T.; Jensen, P. S.; Ulstrup, J. *Chem. Rev.* **2008**, *108*, 2737.
(3) Jadzinsky, P. D.; Calero, G.; Ackerson, C. J.; Bushnell, D. A.; Kornberg, R. D. *Science* **2007**, *318*, 430.
(4) Krüger, D.; Fuchs, H.; Rousseau, R.; Marx, D.; Parrinello, M. *Phys. Rev. Lett.* **2002**, *89*, 186402.
(5) Ohnishi, H.; Kondo, Y.; Takayanagi, K. *Nature* **1998**, *395*, 780.
(6) Wang, Y.; Chi, Q.; Hush, N. S.; Reimers, J. R.; Zhang, J.; Ulstrup, J. *J. Phys. Chem. C* **2011**, *115*, 10630.
(7) Wang, Y.; Chi, Q.; Hush, N. S.; Reimers, J. R.; Zhang, J.; Ulstrup, J. *J. Phys. Chem. C* **2009**, *113*, 19601.
(8) Chi, Q.; Zhang, J.; Ulstrup, J. *J. Phys. Chem. B* **2006**, *110*, 1102.
(9) Wang, Y.; Hush, N. S.; Reimers, J. R. *J. Phys. Chem. C* **2007**, *111*, 10878.
(10) Bilic, A.; Reimers, J. R.; Hush, N. S. *J. Chem. Phys.* **2005**, *122*, 094708.
(11) (a) Wang, Y.; Hush, N. S.; Reimers, J. R. *J. Am. Chem. Soc.* **2007**, *129*, 14532. (b) Reimers, J. R.; Wang, Y.; Cankurtaran, B. O.; Ford, M. J. *J. Am. Chem. Soc.* **2010**, *132*, 8378.
(12) (a) Andreoni, W.; Curioni, A.; Grönbeck, H. *Int. J. Quantum Chem.* **2000**, *80*, 598. (b) Vargas, M. C.; Giannozzi, P.; Selloni, A.; Scoles, G. *J. Phys. Chem. B* **2001**, *105*, 9509.
(13) Yourdshahyan, Y.; Rappe, M. A. *J. Chem. Phys.* **2002**, *117*, 825.
(14) (a) Kondoh, H.; Iwasaki, M.; Shimada, T.; Amemiya, K.; Yokoyama, T.; Ohta, T. *Phys. Rev. Lett.* **2003**, *90*, 066102. (b) Roper, M. G.; Skegg, M. P.; Fisher, C. J.; Lee, J. J.; Dhanak, V. R.; Woodruff, D. P.; Jones, R. G. *Chem. Phys. Lett.* **2004**, *389*, 87. (c) Yu, M.; Bovet, N.; Satterley, C. J.; Bengio, S.; Lovelock, K. R. J.; Milligan, P. K.; Jones, R. G.; Woodruff, D. P.; Dhanak, V. *Phys. Rev. Lett.* **2006**, *97*, 166102.
(15) Molina, L. M.; Hammer, B. *Chem. Phys. Lett.* **2002**, *360*, 264.
(16) Mazzarello, R.; Cossaro, A.; Verdini, A.; Rousseau, R.; Casalis, L.; Danisman, M. F.; Floreano, L.; Scandolo, S.; Morgante, A.; Scoles, G. *Phys. Rev. Lett.* **2007**, *98*, 16102.
(17) (a) Maksymovych, P.; Sorescu, D. C.; Yates, J. T., Jr. *Phys. Rev. Lett.* **2006**, *97*, 146103. (b) Voznyy, O.; Dubowski, J. J.; Yates, J. T.; Maksymovych, P. *J. Am. Chem. Soc.* **2009**, *131*, 12989. (c) Grönbeck, H.; Odelius, M. *Phys. Rev. B* **2010**, *82*, 085416.
(18) Li, F. S.; Zhou, W. C.; Guo, Q. M. *Phys. Rev. B* **2009**, *79*, 113412.
(19) Kautz, N. A.; Kandel, S. A. *J. Am. Chem. Soc.* **2008**, *130*, 6908.
(20) Cossaro, A.; Mazzarello, R.; Rousseau, R.; Casalis, L.; Verdini, A.; Kohlmeyer, A.; Floreano, L.; Scandolo, S.; Morgante, A.; Klein, M. L.; Scoles, G. *Science* **2008**, *321*, 943.
(21) Vericat, C.; Vela, M. E.; Benitez, G.; Carro, P.; Salvarezza, R. C. *Chem. Soc. Rev.* **2010**, *39*, 1805.
(22) Yu, M.; Bovet, N.; Satterley, C. J.; Bengió, S.; Lovelock, K. R. J.; Milligan, P. K.; Jones, R. G.; Woodruff, D. P.; Dhanak, V. *Phys. Rev. Lett.* **2006**, *97*, 166102.
(23) Wang, J. G.; Selloni, A. *J. Phys. Chem. C* **2007**, *111*, 12149.
(24) (a) Chen, W.; Madhavan, V.; Jamneala, T.; Crommie, M. F. *Phys. Rev. Lett.* **1998**, *80*, 1469. (b) Zhang, J.; Chi, Q.; Ulstrup, J. *Langmuir* **2006**, *22*, 6203. (c) Wang, Y.; Hush, N. S.; Reimers, J. R. *Phys. Rev. B* **2007**, *75*, 233416/1.
(25) Marx, D.; Hutter, J. *Ab initio Molecular Dynamics: Basic Theory and Advanced Methods*; Cambridge University Press: Cambridge, 2009.
(26) Kresse, G.; Hafner, J. *Phys. Rev. B* **1993**, *47*, 558.
(27) Perdew, J. P.; Wang, Y. *Phys. Rev. B* **1992**, *45*, 13244.
(28) Jiang, D. E.; Dai, S. *Phys. Chem. Chem. Phys.* **2009**, *11*, 8601.
(29) Lavrich, D. J.; Wetterer, S. M.; Bernasek, S. L.; Scoles, G. *J. Phys. Chem. B* **1998**, *102*, 3456.
(30) Hayashi, T.; Wakamatsu, K.; Ito, E.; Hara, M. *J. Phys. Chem. C* **2009**, *113*, 18795.
(31) Stettner, J.; Winkler, A. *Langmuir* **2010**, *26*, 9659.
(32) Frisch, M. J.; et al. *Gaussian 09*, Revision A.02; Gaussian, Inc.: Pittsburgh PA, 2009.